Indian J Phys (June 2016) 90(6):693–698
DOI 10.1007/s12648-015-0794-5

ORIGINAL PAPER

Studies of structure of calcium–iron phosphate glasses by infrared, Raman and UV–Vis spectroscopies

H J Li[1,2], X F Liang[1,2]*, H J Yu[1,2], D Q Yang[2] and S Y Yang[2]

[1]Analytical and Testing Center, Southwest University of Science and Technology, Mianyang 621010, People's Republic of China

[2]State Key Laboratory Cultivation Base for Nonmetal Composites and Functional Materials, Southwest University of Science and Technology, Mianyang 621010, People's Republic of China

Received: 21 July 2015 / Accepted: 23 September 2015 / Published online: 4 November 2015

Abstract: Glasses in the ternary $CaO–Fe_2O_3–P_2O_5$ system were prepared and studied by means of density, differential scanning calorimetry, infrared, Raman and UV–Vis spectroscopies. The results showed that density and molar volume in the glass system decreased with increasing substitution of CaO for Fe_2O_3. The variation of glass transition temperature and thermal stability was strictly related to the nature of bonding in the vitreous network. Spectroscopic analysis showed that substitution of CaO for Fe_2O_3 induced an evolution of structural units from pyrophosphate to metaphosphate species indicating the polymerization of phosphate chains and the decrease of non-bridging oxygen concentrations. With increasing substitution of CaO for Fe_2O_3 The P–O–Ca linkage and ($P–O^- Ca^{2+} {}^-O–P$) chains participated in the glass network by replacing P–O–Fe bonds. The absorption band of the P–O–Ca stretching mode in the glasses with high CaO content (≥32 mol%) was assigned at around 1084 cm^{-1}. The absorption edge would fall in the region between 332 and 420 nm which are the absorption bands of Fe^{3+} ions.

Keywords: Calcium oxide; Molar volume; Raman spectroscopy; UV–Vis spectroscopy

PACS Nos.: 32.30.Jc

1. Introduction

Phosphate glasses have been proposed as good candidates for vitrifying high level nuclear wastes (HLW) due to their lower melting temperatures, higher waste loading and waste compositional flexibility [1, 2]. However, poor chemical durability of phosphate glasses and high crystallization tendency of their melts led to the exclusion of phosphate glasses from the pool of potential host matrices in the early 1970s [1–3]. Phosphate glasses are also important for their various interesting properties [4–8].

Several studies have shown that chemical durability of the glasses can be improved by the addition of one or more oxides such as CaO, TiO_2, PbO, ZnO, CuO, Al_2O_3 and Fe_2O_3 [2, 9–12]. Among these additions, low cost and environmental friendly Fe_2O_3 enhances chemical durability dramatically. The binary iron phosphate glass with an approximate composition of $40Fe_2O_3–60P_2O_5$ (mol%) forms more hydration resistant P–O–Fe bonds by replacing more easily hydrated P=O bonds and P–O–P bonds, leading to better chemical durability [2, 3]. CaO is another oxide which is usually added to phosphate glasses to improve chemical durability. The presence of CaO, acting as a network modifier, imparts wider glass forming region and lower viscosity [9, 12, 13]. Donald et al. [14] have indicated that calcium phosphate has appeared to be a viable starting material for the immobilization of a variety of actinide-, fluoride- and chloride-containing wastes.

Metcalfe et al. [9] have measured that dissolution rates of the ternary $CaO–Fe_2O_3–P_2O_5$ glass gravimetrically on monolithic samples for HLW waste. The results indicate that the glasses have more favorable properties on corrosion resistance than the binary iron phosphate glass ($40Fe_2O_3–60P_2O_5$, mol%). However, a little systematic work has been conducted to identify the change of the structural units in such glasses and correlate these changes with the non-bridging oxygens (NBOs) and bridging oxygens (BOs) in the glass network. Phosphate glasses can be

*Corresponding author, E-mail: XFLiang@swust.edu.cn

prepared with a range of structures, from a cross-linked network of Q^3 tetrahedra (vitreous P_2O_5) to polymer-like metaphosphate chains of Q^2 tetrahedra to 'invert' glasses based on small pyro- (Q^1) and orthophosphate (Q^0) anions, depending on the [O]/[P] ratio as set by glass composition [11, 15].

In the present paper, the structural modifications in calcium–iron phosphate glasses obtained by replacing of Fe_2O_3 with CaO have been investigated by means of density, differential scanning calorimetry (DSC), infrared, Raman and UV–Vis spectroscopies.

2. Experimental details

$CaO–Fe_2O_3–P_2O_5$ glasses were investigated for the composition $xCaO–(40–x)Fe_2O_3–60P_2O_5$ for x = 0–40 mol% CaO. Glasses were prepared using CaO, Fe_2O_3 and $NH_4H_2PO_4$ as the starting materials. The accurately weighed batches were introduced in alumina crucibles. In order to prevent the excess boiling and consequent spillage, water and ammonia in ammonium phosphate monobasic were removed initially by preheating it at 220 °C for about 2 h and then the temperature was raised to 1200 °C (heating rate was 10 °C min^{-1}), and samples were melted at 1200 °C for 3 h. The melts were then quenched to room temperature in order to produce vitreous samples. Samples for property measurements were ground to give fine powder.

The density (ρ) of each glass was measured at room temperature using the Archimedes method with water as an immersing liquid. The sample weights varied between 3 and 4 g, and the measured densities were reproducible within 0.03 g cm^{-3}. The molar volume (V_m) was calculated using the relation $V_m = \sum(x_i M_i)/\rho$, where x_i is the molar fraction and M_i is the total molecular weight of the component. The composition of the prepared glass was used for the calculation of V_m. The glass transition temperature (T_g) and first crystallization temperature (T_r) were measured on DSC by utilizing a SDT Q600 instrument (TA, USA) in a flowing air atmosphere at a heating rate of 20 °C min^{-1}. The temperature was scanned over a range from room temperature to 800 °C and the estimated error in T_g and T_r were ±2 °C.

X-ray diffraction (XRD) analysis was performed on samples employing a X-ray diffractometer (PANalytical X'Pert PRO, The Netherlands). The 2θ scans were made between 5° and 80° with step width of 0.03° and utilized Cu Kα radiation (λ = 1.5405 Å). The infrared spectra of the samples were measured from 400 to 2000 cm^{-1} using a Spectrum One FT–IR spectrometer (Perkin Elmer, USA) and the KBr standard pellet method. Glass pellets were prepared by mixing about 2 mg powder with 200 mg dried KBr powder and compressing the resulting mixture in an evacuated die. The accuracy of this technique was estimated to be ±0.5 cm^{-1}. Raman spectra at 400–1600 cm^{-1} were collected from glass powders using the InVia Raman Microscope (Renishaw, UK) at room temperature. The Raman spectra were excited by 514.5 nm light from an argon ion laser. The spectral resolution was about 1–2 cm^{-1} and the wavenumber accuracy was 0.2 cm^{-1}. Six multiple measurements per sample were done to check for the potential micron-range heterogeneity and for the effects of sample orientation.

The diffuse reflectance spectra of the powdered glass samples were recorded at room temperature in the 200–800 nm range up to a resolution of 0.3 nm using a UV–Vis near-infrared spectrometer (UV-3150, Shimadzu, Tokyo, Japan) with the ISR-3100 integrating sphere attachment.

In the limiting case of an infinitely thick sample, thickness and sample holder has no influence on the value of reflectance (R). In this case, the Kubelka–Munk equation at any wavelength becomes [16, 17]:

$$F(R\infty) = (1 - R\infty)^2/(2R) \quad (1)$$

$F(R\infty)$ is the so-called remission or Kubelka–Munk function, where $R\infty = R_{sample}/R_{standard}$. The following relational expression proposed by Tauc et al. [15, 18] was used

$$\alpha h\nu = C_1(h\nu - E_g)^{\frac{1}{2}} \quad (2)$$

where h is Planck's constant, ν is frequency of vibration, α is absorption coefficient, E_g is band gap and C_1 is proportional constant.

The acquired diffuse reflectance spectrum was converted to Kubelka–Munk function. Thus, the vertical axis was converted to quantity $F(R\infty)$, which was proportional to the absorption coefficient. The α in the Tauc equation is substituted with $F(R\infty)$. Thus, in the actual experiment, the relational expression becomes [16]:

$$[F(R\infty)h\nu]^2 = C_2(h\nu - E_g) \quad (3)$$

Therefore, obtaining $F(R\infty)$ from Eq. (1) and plotting the $[F(R\infty)h\nu]^2$ against hν, the band gap E_g of a powder sample can be extracted easily.

3. Results and discussion

3.1. XRD, density and thermal properties

The X-ray diffraction patterns of the $xCaO–(40–x)Fe_2O_3–60P_2O_5$ glasses system show no sharp peaks ensuring amorphous nature of the samples. All prepared glass

samples are homogeneous, and their glassy state has been checked by X-ray diffraction. The obtained compositional range corresponding to glass forming regions in the ternary $CaO–Fe_2O_3–P_2O_5$ system was described by Brow et al. [19].

The density, mole volume and DSC parameters of the studied glasses are given in Table 1. The density of glasses decreases from 3.06 to 2.57 g/cm^3 and the molar volume decreases slightly when Fe_2O_3 is replaced by CaO. Density of glasses decreases with increasing CaO substitution, which is due to the smaller atomic weight of calcium (40 g/mol) compared to iron (56 g/mol). It is well known that the change of molar volume is associated with the change of the glass structure. The decrease in molar volume is ascribed to a decrease in the number of non-bridging oxygens [18]. This decrease in molar volume indicates that the phosphate glass network becomes more compact.

For the glass system, the glass transition temperature (T_g) and the first crystallization peak (T_r) increase for glasses containing $\leq$24 mol% CaO, while T_g and T_r decrease for glasses containing $\geq$24 mol% CaO (Table 1). The variation of glass transition temperature is strictly related to the nature of bonding in the vitreous network. The difference between the glass transition temperature (T_g) and the onset crystallization temperature (T_r), $\Delta T = T_r - T_g$, has been frequently used as a accurate estimate of glass thermal stability [20]. ΔT values in the glasses increase as Fe_2O_3 is replaced by CaO (Table 1). It indicates that glass thermal stability improves with increasing substitution of CaO for Fe_2O_3.

3.2. Infrared spectroscopy

FT-IR spectra together with vibration frequency and their identifications for the $xCaO–(40–x)Fe_2O_3–60P_2O_5$ glasses system are shown in Fig. 1. As Fe_2O_3 is replaced by CaO, the most notable change is that the band at $\sim$1268 cm^{-1} appears for glass containing 24 mol% CaO and shifts to the high frequency band at $\sim$1304 cm^{-1} with increasing substitution of CaO. The most intense peak in the spectra has an obvious red shift from 1111 cm^{-1} up to 1070 cm^{-1}. However, there is a slight increase in frequency and decrease in intensity beyond 24 mol% CaO. In addition, the band at 517 cm^{-1} shifts to the low frequency band at 506 cm^{-1}, and a weak band at $\sim$491 cm^{-1} appears. The assignment of the IR absorption bands for the studied $40CaO–60P_2O_5$ glasses is similar to that reported in the literature for different alkali phosphate glasses [1, 21].

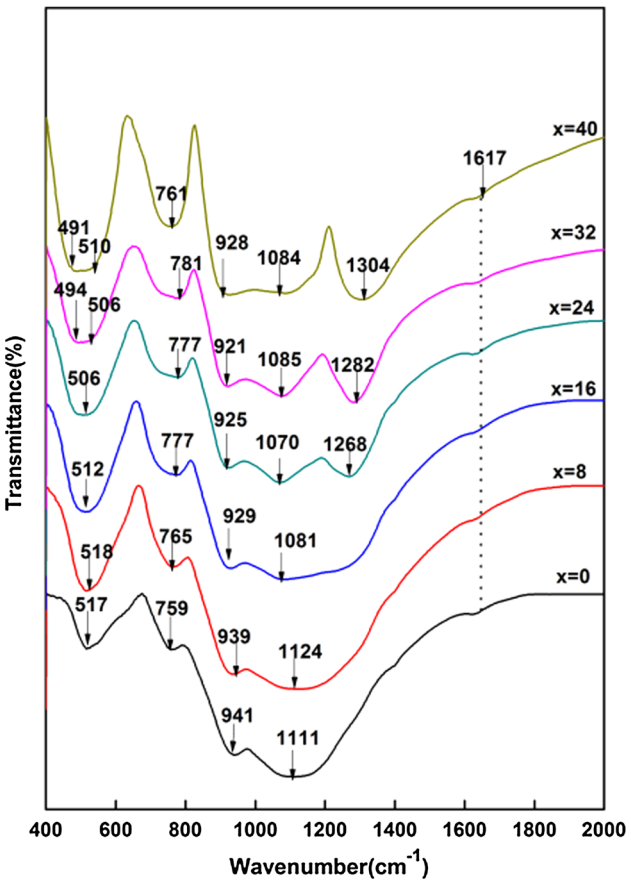

Fig. 1 IR spectra of different composition of $xCaO–(40–x)Fe_2O_3–60P_2O_5$ glasses. Different peaks are shown by *arrows*

The IR spectra of the parent $40Fe_2O_3–60P_2O_5$ glass in the glasses system reveal five bands at $\sim$1617, $\sim$1111, $\sim$941, $\sim$759 and $\sim$517 cm^{-1}, respectively. The band at

Table 1 Composition, density (ρ), molar volume (V_m), DSC parameters and band gap (E_g) of $xCaO–(40–x)Fe_2O_3–60P_2O_5$ glasses

Sample identification (mol%)	O/P	ρ (g cm^{-3})	V_m (cm^3 mol^{-1})	T_g (°C)	T_r (°C)	T_r-T_g (°C)	E_g (eV)
x = 0	3.50	3.06	48.66	517	596	79	2.90
x = 8	3.37	2.98	47.24	543	623	80	3.04
x = 16	3.23	2.91	45.55	563	646	83	3.09
x = 24	3.10	2.81	44.13	576	660	84	3.11
x = 32	2.97	2.71	42.76	570	657	87	3.13
x = 40	2.83	2.57	41.94	532	628	96	4.14

$\sim$1617 cm^{-1} reflected water-bending mode [2, 20]. The band at $\sim$1111 cm^{-1} is assigned to the asymmetric stretch of $(PO_3)^{2-}$ group in Q^1 units [22], while the absorption bands at $\sim$941 and $\sim$517 cm^{-1} correspond to the symmetric modes of P–O–P bonds in the Q^1 units [22] and fundamental frequencies $(PO_4)^{3-}$ of Q^0 units [2, 20], respectively.

As Fe_2O_3 is replaced by CaO, the absorption bands in the region 900–1300 cm^{-1} for the glasses system become wider and the the new band at $\sim$1268 cm^{-1} appears for glass containing $\geq$24 mol% CaO, which is assigned to the asymmetric stretching mode of the $(PO_2)^-$ group in Q^2 units [20, 22]. It may be due to the formation of the (P–O^- Ca^{2+} $^-$O–P) ionic cross-links between two different phosphate chains [12, 23]. The bond strengthens the crosslinking of the glass network, with consequent increases in T_g. The new band at $\sim$1304 cm^{-1} is assigned to the asymmetric stretching vibration of P=O bonds [22]. It is concluded that calcium ions act as a glass modifier and occupy the positions between P–O–P layers, leading to the increase of the P=O bonds. Similar behavior in Fe_2O_3–PbO–P_2O_5 glasses has been observed by Doweidar et al. [24].

In addition, the new band at $\sim$1070 cm^{-1} is assigned to the asymmetric stretch of $(PO_4)^{3-}$ tetrahedra (P–O^- ionic group) in Q^0 units [25, 26]. Shih et al. [27] have shown that the absorption band near 1080 cm^{-1} in the IR spectra of CuO–Na_2O–P_2O_5 glasses is associated with the stretching mode of the P–O–Cu linkage by the replacing P–O^-. Therefore, we suggest that the band at $\sim$1084 cm^{-1} in the 40CaO–60P_2O_5 glass may be associated with the P–O–Ca linkage, which may lead to the increase of frequency in the IR spectra of the glass system for CaO $\geq$ 24 mol%. The decrease of T_g in Table 1 can be due to the formation of the P–O–Ca linkage by the replacing P–O–Fe bonds with increasing substitution of CaO for Fe_2O_3. The low frequency band at $\sim$491 cm^{-1} appears, which may be assigned to the harmonics of bending vibration of O=P–O linkages in Q^3 units [28]. These changes can be attributed to the depolymerization of pyrophosphate chains when the O/P ratio decreases (Table 1).

3.3. Raman spectroscopy

Raman spectra of the studied glasses are shown in Fig. 2. In the Raman spectra of the glasses system, the prominent band at $\sim$1092 cm^{-1} shifts markedly to the high frequency band at $\sim$1173 cm^{-1} and the new band at $\sim$1293 cm^{-1} appears with increasing substitution of CaO. In addition, the bands at $\sim$767 and $\sim$952 cm^{-1} shift gradually to the low frequency bands at $\sim$705 and $\sim$879 cm^{-1}, respectively.

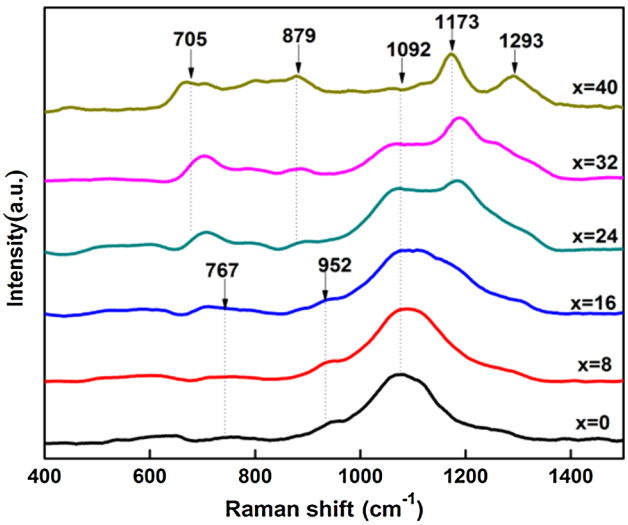

Fig. 2 Raman spectra of different composition of xCaO–(40–x)Fe_2O_3–60P_2O_5 glasses

In Fig. 2, the Raman spectra of the 40Fe_2O_3–60P_2O_5 glass reveals three bands at $\sim$1092, $\sim$952 and $\sim$767 cm^{-1}, respectively. The most intense peak at $\sim$1092 cm^{-1} in the Raman spectra is assigned to the symmetric stretching mode of $(PO_3)^{2-}$ bonds in Q^1 units [2]. With increasing substitution of CaO, the band shifts markedly to the high frequency band at $\sim$1173 and $\sim$1293 cm^{-1}, which correspond to the asymmetric stretching mode of the $(PO_2)^-$ group in Q^2 units and the P=O symmetric stretching [12, 28], respectively. The shift of these bands indicates that the metaphosphate (Q^2) species dominate the structure of the CaO–P_2O_5 glass and substitution of CaO for Fe_2O_3 depolymerizes the pyrophosphate groups to form the metaphosphate long chains or rings.

The bands at $\sim$952 and $\sim$767 cm^{-1} correspond to the asymmetric stretching mode of $(PO_4)^{3-}$ in Q^0 units [11] and the symmetric stretching mode of P–O–P bonds in Q^1 units [2, 11], respectively. These bands shift to the lower frequency at $\sim$879 and $\sim$705 cm^{-1} with increasing CaO substitution. The two bands can correspond to the symmetric stretching mode of P–O–P bonds in Q^2 units [11]. Similar bands have been observed in the Raman spectra from the metaphosphate glasses [10, 29]. Therefore, calcium oxide in the studied glasses acts as a network modifier and incorporates into the network with increasing CaO for Fe_2O_3 substitution.

Both variations in Raman and IR spectra demonstrates the concomitance of Q^0, Q^1 and Q^2 species and the variation of dominant structural units from pyrophosphate to metaphosphate species, resulting in the increase of the average phosphate chain length and the decrease of non-bridging oxygen concentrations. The change of dominant

structural units may lead to the increase of the thermal stability (ΔT). Since the field strength of the iron ion (Fe^{3+} and Fe^{2+}) is higher than that of Ca^{2+}, the lower Ca–O bond force constant leads to the shift of structural units.

3.4. UV–Vis spectroscopy

In order to get further into the structure of the investigated glasses, diffuse reflectance UV–Vis (DR UV–Vis) spectra of the studied glasses are presented in Fig. 3. The DR spectra of the glasses system shows that the reflectivity increases in the visible region as Fe_2O_3 is replaced by CaO in the glass composition. Parent iron phosphate glass is black, and the black coloration become shallower with increasing substitution of CaO for Fe_2O_3. Calcium phosphate glasses are colourless. It is expected to result in the increase of the reflectivity in the visible region.

The three absorption bands are observed in the parent $40Fe_2O_3$–$60P_2O_5$ glasses at around 324 and 352 nm in the ultraviolet region and at around 540 nm in the visible region, and the three bands decrease in intensity or disappear with increasing CaO substitution. A new band at 235 nm in the $40CaO$–$60P_2O_5$ glass appears.

Iron exists in the $40Fe_2O_3$–$60P_2O_5$ glass as Fe^{2+} ions (occupies usually octahedral positions and plays the network modifier role) and Fe^{3+} ions (occupies both tetrahedral and octahedral positions with the network former role) [30]. Some authors [31, 32] have shown that the bands centered in the 325–450 nm region are due to the presence of the Fe^{3+} ions, the UV–Vis bands associated with the Fe^{2+} ions are located in the ultraviolet region due to the iron–oxygen charge transfer and in the visible range in the 450–550 nm region. The absorption band at around 352 nm is due to the d–d transitions of the Fe^{3+} ions. The d–d transitions of the Fe^{3+} ions decrease with increasing CaO content. The weak absorption bands at 324 nm and 540 nm is due to a strong Fe–O charge transfer derived to the Fe^{2+} and Fe^{3+} ions and the d–d transitions of the Fe^{2+} ions in the near infrared region, respectively [31, 33]. Then, the new band centered at 235 nm would be due to the charge transfer transition of Ca–O in the $40CaO$–$60P_2O_5$ glass (Fig. 3) [34]. The increase of CaO content for Fe_2O_3 substitution produces a shift of the fundamental absorption edge from 420 nm to a shorter wavelength at about 332 nm, indicating the decrease of disorder degree of the glass system. The region of absorption edge is the absorption bands of Fe^{3+} ions.

Kubelka–Munk transformed reflectance spectra of the studied glasses are shown in Fig. 4. From the extrapolation of the linear portion of these spectra, the values of the band gap (E_g) have been determined. The value of the band gap in the glasses system is found to decrease with increasing CaO content (Table 1). The modifications in the band gap energy can be understood in terms of the variation in non-bridging oxygen concentrations in the glass network. Some authors [35, 36] have attributed the increase of the band gap energy to the decrease of the amount of NBOs. The results are in agreement with Raman spectra and density data. The non-bridging orbitals have higher energies than the bonding orbitals [37]. The non-bridging oxygen ions contribute to the valence band maximum. Accordingly, addition of CaO causes a decrease in non-bridging oxygen concentration, which increases the band gap energy.

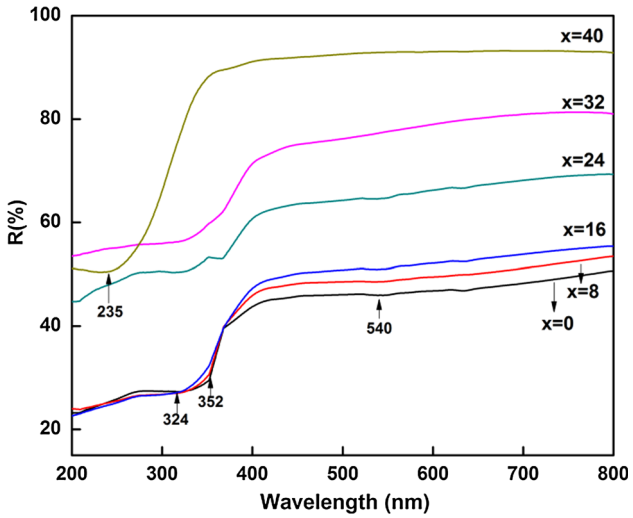

Fig. 3 Diffuse reflectance spectra of different composition of xCaO–(40–x)Fe_2O_3–$60P_2O_5$ glasses

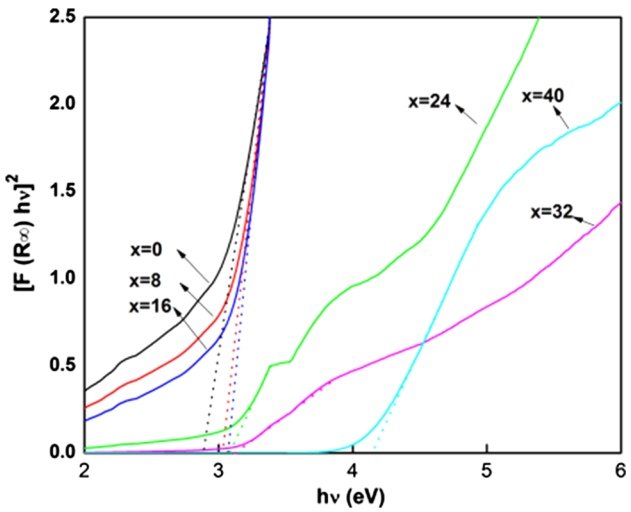

Fig. 4 Kubelka–Munk transformed reflectance spectra of different composition of xCaO–(40–x)Fe_2O_3–$60P_2O_5$ glasses

4. Conclusions

The ternary glasses in the system $xCaO–(40–x)Fe_2O_3–60P_2O_5$ with 0–40 mol% CaO have been obtained. As Fe_2O_3 is replaced by CaO in the glass system, density and molar volume of glasses decrease. It indicates that the phosphate glass network becomes more compact. Infrared and Raman spectra indicate that substitution of CaO for Fe_2O_3 creates the P–O–Ca linkage and ($P–O^-$ Ca^{2+} $^-O–P$) chains, resulting in the variation of dominant structural units from pyrophosphate to metaphosphate species. The absorption band is assigned the P–O–Ca stretching mode in the glasses with high CaO content at around 1084 cm^{-1}. UV–Vis spectra show that the absorption edge falls in the region between 332 and 420 nm in the absorption bands of Fe^{3+} ions. The increase of the band gap energy with increasing CaO substitution is attributed to the decrease of non-bridging oxygen concentration. The variation of these bonds with increasing CaO substitution leads to the change of T_g and thermal stability.

Acknowledgments This work was supported by the Science Foundation of Southwest University of Science and Technology (11zx7157), the Scientific Research Fund of SiChuan Provincial Education Department (14ZA0105, 14ZD1122) and Postgraduate Innovation Fund Project by Southwest University of Science and Technology (14ycx018).

References

[1] R O Omrani, S Krimi, J J Videau, I Khattech, A E Jazouli and M Jemal *J. Non-Cryst. Solids* **389** 66 (2014)
[2] B Qian, X F Liang, S Y Yang, S He and L Gao *J. Mol. Struct.* **1027** 31 (2012)
[3] M Karabulut, G K Marasinghe, C S Ray, D E Day, O Ozturk and G D Waddill *J. Non-Cryst. Solids* **249** 106 (1999)
[4] S Kabi and A Ghosh *Solid State Ion.* **262** 778 (2014)
[5] S Shaw and A Ghosh *EPL Europhys. Lett.* **100** 66003 (2012)
[6] S Shaw and A Ghosh *J. Phys. Chem. C* **116** 24255 (2012)
[7] S Kabi and S Ghosh *Solid State Ion.* **187** 39 (2011)
[8] A Pan and A Ghosh *J. Chem. Phys.* **112** 1503 (2000)
[9] P A Bingham and R J Hand *Mater. Res. Bull.* **43** 1679 (2008)
[10] X Y Li, H M Yang, X L Song and Y Wu *J. Non-Cryst. Solids* **379** 208 (2013)
[11] R K Brow, D R Tallant, S T Myers and C C Phifer *J. Non-Cryst. Solids* **191** 45 (1995)
[12] A M B Silva, R N Correia, J M M Oliveira and M H V Fernandes *J. Eur. Ceram. Soc.* **30** 1253 (2010)
[13] Z Wu, C S Ray and P Hrma *J. Non-Cryst. Solids* **241** 1 (1998)
[14] I W Donald, B L Metcalfe, S K Fong, L A Gerrard, D M Strachan and R D Scheele *J. Nucl. Mater.* **361** 78 (2007)
[15] R K Brow *J. Non-Cryst. Solids* **263** 1 (2000)
[16] J Zheng, Z Q Liu, X Liu, X Yan, D D Li and W Chu *J. Alloys Compd.* **509** 3771 (2011)
[17] F Yakuphanoglu *J. Alloys Compd.* **507** 184 (2010)
[18] M Rada, E Culea, S Rada, A Bot, N Aldea and V Rednic *J. Non-Cryst. Solids* **358** 3129 (2012)
[19] R K Brow, D R Tallant, W L Warren, A McIntyre and D E Day *Phys. Chem. Glasses* **38** 300 (1997)
[20] B Qian, X F Liang, C L Wang and S Y Yang *J. Nucl. Mater.* **443** 140 (2013)
[21] Y M Moustafa and K El-Egili, *J. Non-Cryst. Solids* **240** 144 (1998)
[22] B Qian, S Y Yang, X F Liang, Y M Lai, L Gao and G F Yin *J. Mol. Struct.* **1011** 153 (2012)
[23] B C Bunker, G W Arnold and J A Wilder *J. Non-Cryst. Solids* **64** 291 (1984)
[24] H Doweidar, Y M Moustafa, K El-Egili and I. Abbas *Vib. Spectrosc.* **37** 91 (2005)
[25] P Pascuta, G Borodi, A Popa, V Dan and E Culea *Mater. Chem. Phys.* **123** 767 (2010)
[26] L Baia, M Baia, W Kiefer, J Popp and S Simon *Chem. Phys.* **327** 63 (2006)
[27] P Y Shih, J Y Ding and S Y Lee *Mater. Chem. Phys.* **80** 391 (2003)
[28] H J Li, X F Liang, C L Wang, H J Yu, Z Li and S Y Yang *J. Mol. Struct.* **1067** 154 (2014)
[29] J J Hudgens, R K Brow, D R Tallant and S W Martin *J. Non-Cryst. Solids* **223** 21 (1998)
[30] X Yu, D E Day, G J Long and R K Brow *J. Non-Cryst. Solids* **215** 21 (1997)
[31] S Rada, A Dehelean, M Stan, R Chelcea and E Culea *J. Alloys Compd.* **509** 147 (2011)
[32] L Rus et al. *J. Non-Cryst. Solids* **402** 111 (2014)
[33] S M Abo-Naf, M S El-Amiry and A A Abdel-Khalek *Opt. Mater.* **30** 900 (2008)
[34] H Tanaka, T Okumiya, S Ueda, Y Taketani and M Murakami *Mater. Res. Bull.* **44** 328 (2009)
[35] S Rada, M Rada and E Culea *J. Non-Cryst. Solids* **357** 62 (2011)
[36] S Rada et al. *Electrochim. Acta* **109** 82 (2013)
[37] M Rada, E Culea, S Rada, A Bot, N Aldea and V Rednic *J. Non-Cryst. Solids* **358** 3129 (2012)